Optimized preparation of lysozyme loaded dextran-chitosan nanoparticles using D-optimal design

Taraneh Hadi Esfahani[1], Amir Azadi[2], Niloofar Joodi[1,] Reza Ahangari Cohan[3], Iman Akbarzadeh [4], Haleh Bakhshandeh [3] [*]

[1] School of Pharmacy, Nanotechnology Research Centre, Zanjan University of Medical Sciences, Zanjan, Iran
[2] Pharmaceutical Research Center, Shiraz University of Medical Sciences, Shiraz, Iran
[3] Nanobiotechnology Department, New Technologies Research Group, Pasteur Institute of Iran, Tehran, Iran
[4]Department of Chemical and Petroleum Engineering, Biotechnology Research Cen ter, Sharif University of Technology, Tehran, Iran

***Corresponding author:** Haleh Bakhshandeh, Nanobiotechnology Department, New Technologies Research Group, Pasteur Institute of Iran, Tehran, Iran. Email: h.bakhshandeh@gmail.com*

ABSTRACT

In this study, optimized conditions were investigated using response surface methodology for the preparation of lysozyme loaded dextran-chitosan nanoparticles. Nanoparticles were prepared using polyelectrolyte complexation method. Relevant factors including polymer ratio, protein concentration, stirring rate, and temperature were considered and the effects of these factors on size, polydispersity index (PDI), entrapment efficiency (EE), and zeta potential of the nanoparticles were investigated. The optimum condition for the nanoparticle preparation was found at chitosan/dextran ratio of 0.37, 1.5 mg/mL with 1600 rpm stirring at 32 °C. The particle size, PDI, encapsulation efficiency, and zeta potential at the optimum conditions were 188.5 nm, 0.287, 84.6 %, and -18.76 mv, respectively. This study revealed that encapsulation of positively charged lysozyme, as a model protein, within negatively charged dextran-chitosan nanocarriers improve the loading capacity and the release properties under physiological conditions.

*Keywords***:** Polyelectrolyte complexation; chitosan; dextran sulfate; nanoparticle; D-optimal design

INTRODUCTION

With advances in biotechnology, numerous therapeutic proteins are approved for treatment of cancer, diabetes, multiple sclerosis, infections, rheumatoid arthritis, leukemia, and growth deficiencies [1]. Nonetheless, noninvasive delivery routes of proteins are not achieved successfully so far. Oral administration of proteins is highly challenging due to poor stability of proteins at low pH of gastric fluid and poor permeation through gastrointestinal membranes. Also, degradation of protein by proteases in the lung and metabolic enzymes in the nasal mucosal cavity and various clearance mechanisms limit bioavailability of proteins in pulmonary and nasal delivery routes [2]. Therefore, despite of enormous efforts for the improving of noninvasive delivery systems, parenteral routes are still the main routes for clinical administration of therapeutic proteins. Additionally, systematic administration of therapeutic proteins suffers from the poor stability of proteins, and therefore, short *in vivo* half-life usually in the range of a few minutes to a few hours. These limitations lead to frequent dose administrations, lower therapeutic effectiveness, and poor patient compliance [3,4].

Encapsulation have considered as a potent approach to overcome the protein delivery limitations. Encapsulation improves the protein stability and extends plasma half-life by protecting the protein from the enzymatic degradation. It also provides a prolonged and/or controllable release of proteins from the carrier. Clinically, it increases the efficacy while reduces side effects, and enhances patient compliance by reducing administration frequency [3-5]. Among carrier systems, natural polymeric nanoparticles offer unique advantages over others such as subcellular size, high biocompatibility, biodegradability, availability, and low cost [6]. Polyelectrolyte complexation (PEC), also known as coacervation, is one of the best methods for preparing nanoparticles from natural polymers. PEC is mainly occurred by ionic interaction between immiscible dense and dilute liquid phases that differ in protein and polyelectrolyte concentrations [7]. Protein-loaded nanoparticles could be easily prepared by PEC process under mild conditions without reaching high temperatures or sonication [8]. This method yields nanoparticles with high surface charge density that efficiently adsorb oppositely charged protein through electrostatic interactions. Many investigations have been revealed preparation parameters such as pH, polymers mass ratio, polymers charge ratio,

and ionic strength could affect the properties of such nanoparticles [9-12].

In the current study, chitosan and dextran were used for nanoparticle preparation using PEC method. These polymers are capable of forming complexes via electrostatic interactions. As aforementioned, the process occurs in a very mild condition in an aqueous media without using organic solvent, surfactant, high tension force or heat. Therefore, this method is considered as a suitable technique for encapsulation of sensitive drugs such as peptides and proteins. Lysozyme was also used as a model protein because of unique physicochemical properties such as a high isoelectric point, water solubility, as well as variety of biomedical applications including antibacterial activity and biomarkers [13-17]. Also, the optimum condition for preparation of protein-loaded nanoparticles was achieved via D-optimal design.

MATERIALS AND METHODS

Materials

Chitosan with 89 % degree of deacetylation was purchased from Primex (Karmoy, Norway). Dextran sulfate (Mw of 500 kDa) and zinc sulfate heptahydrate were obtained from Sigma-Aldrich (St. Louis, MO, USA). Lysozyme was purchased from Cinnagen (Iran). BCA kit for total protein

measurements was obtained from Pierce Company. All other reagents were analytical grade.

Chitosan depolymerization

Two grams of low molecular weight chitosan was dissolved in 100 mL of 6 % acetic acid. Then, 10 mL of sodium nitrite with a concentration of 2.7 mg/mL was prepared in deionized water and added to the solution. The mixture was stirred for 1 hour at room temperature. After that, chitosan was precipitated by adding 4 M NaOH (up to pH 9). The precipitate was filtered on a Buchner funnel and washed three times with pure acetone. Dry mass was dissolved in the 0.1 M acetic acid and the solution was dialyzed twice, each time for 90 minutes and then for an overnight in 1 liter of deionized water. Depolymerized chitosan was frozen in a dialysis bag and lyophilized under vacuum condition at -30 °C and 0.01 millibar pressure (EYELA, FDU-2100, Japan) [18].

Molecular weight determination of depolymerized chitosan

The molecular weight of depolymerized chitosan was examined by static light scattering (SLS) method using a particle size analyzer (Zetasizer Nano ZS, MALVERN, UK)[19,20]. Different concentrations of depolymerized chitosan (1, 2, 3, 4, and 5

58

mg/mL) were prepared and light scattering intensities were measured and plotted in Debye plot. The molecular weight of depolymerized chitosan was obtained from the intercept of Debye plot.

Experimental design

A combinatorial systematic approach was used for optimization of nanoparticle preparations. For this purpose, D-optimal method was used to evaluate the relationship between the variables and their responses and also determine the optimum condition for the process [21,22]. Relevant factors including polymer ratio, protein concentration, stirring rate, and temperature were considered as the main variables and the selected responses were final Z-average size of the particles, PDI, and entrapment efficiency (EE) (Table 1). Our design presented a statistical model to describe the effects of preparation conditions on the responses. A stepwise regression model was utilized to fit the polynomial model to the data. A lack of fit test with the analysis of variance (ANOVA) model, a plot of the residuals versus predicted values, leverage and a graphical demonstration of the experimental versus predicted values demonstrated the suitability of the model. Also, the qualities of the fitted models were examined by the coefficient of determination, R^2. The differences between responses were

analyzed statistically using the ANOVA. The best model fitting to the test data via D-optimal design was assessed by Design-Expert statistical software (version 6.0.10, Stat-Ease Inc., Minneapolis, USA). The normal probability plot and Cook's distance were applied to the detection of outliers. Response surfaces plots were prepared to analyze the optimum conditions for the dependent variables. The design matrix and responses were shown in (Table 2). Twenty five experiments (15 minimum model points, 5 points to estimate lack of fit and 5 replicate points) were designed in triplicate. In addition, multi-criteria optimization was used based on desirability index of Derringer using design expert software version 6.0.10. The model adequacy was also verified by five additional experiments using the predicted optimum conditions.

Preparation of lysozyme-loaded nanoparticles

A pre-determined amount of dextran sulfate and lysozyme were dissolved in deionized water to obtain the desired concentration needed according to the experimental design. Chitosan was dissolved in acetic acid buffer (pH adjusted to 6) at concentration of 0.1 % w/v. As a typical procedure, in each run, 600 µL of lysozyme containing solution was added to the 800 µL of dextran sulfate

solution and stirred for 30 min at the specified stirring rate. Then, 1.6 mL of chitosan solution was added dropwise to the mixture. Finally, 100 µL of zinc sulfate solution (1M) was added and stirred for another 30 min. Each prepared sample was centrifuged (14000 g, 45 min, at 4 ˚C) twice. The supernatant was assayed for the encapsulation efficiency and the prepared nanoparticles were subjected to characterization and release tests [23-25].

Characterization of lysozyme-loaded nanoparticles

Particle size, PDI, and surface charge measurements

The mean particle size and PDI were determined by dynamic light scattering employing a particle size analyzer (Zetasizer Nano ZS, MALVERN, UK). Samples were diluted with deionized water to prepare an appropriate concentration. The surface charge (zeta potential) of the nanoparticles was determined by laser Doppler electrophoresis using the same instrument. Each measurement was performed triplicate.

Entrapment efficiency

To determine the encapsulation efficiency, the samples were centrifuged (14000 g for 45 min, 4 °C) and the supernatants were separated. Then, protein concentration

measurements were carried out by BCA assay in triplicate. The optical density of the samples was read at 562 nm with a microplate reader (Biotek Elx800, USA). Nine standard solutions were used to prepare the standard curve. The percentage of encapsulation efficiency was finally calculated according to equation 1.

Entrapment Efficiency (%) = (weight of protein found loaded / weight of protein input) * 100 (Equation 1)

Morphology

The shape of nanoparticles and aggregation phenomena were studied by Scanning Electron Microscopy (SEM, xl30; Philips Eindhoven the Netherlands) and Atomic Force Microscopy (AFM, JPK Instruments Co., Germany). For SEM, one drop of diluted nanosuspension was mounted on metal stubs and coated under vacuum using a sputter coater (SCD 005; bad Tec, Balzers, Switzerland). For AFM, 10 µL of 50 fold diluted nanoparticles were placed on a cleaved mica sheet. The sample was placed at room temperature for 10 min and then washed by 50 µL deionized water. Then, it was dried by a gentle flow of air at room temperature. The cantilever was HYDRA6V-100N, pyramidal tip shape with force constant of 0.292 N/m and the resonance

60

frequency of 66 kHz (Applied Nanostructures Inc., Mountain View, CA). Processing of topographic images was performed by JPK data processing software (version spm-3.4.15, JPK Instruments Co., Germany).

In vitro release study

Twenty milligrams of prepared nanoparticles were dispersed in a microtube containing 1 mL phosphate buffer (adjusted to pH 7.4). The sealed tube was then placed in a shaker incubator at 37 °C and 90 rpm. At specific time intervals, the release medium was centrifuged at 1500 g at 4 °C for 15 min. The supernatants were then subjected to the protein measurements using BCA assay and

the sediment was resuspended with the same amount of phosphate buffer [12].

RESULTS

Chitosan depolymerization

Depolymerization was performed to obtain chitosan with low molecular weight because of its valuable properties such as solubility in different pH, the creation of smaller nanoparticles with high EE [26]. The molecular weight was determined by SLS method which is a reliable method for molecular weight determination of proteins and polymers. MW of the polymer was obtained 12.4 kDa from the intercept of Debye plot (Figure 1).

Table 1. Variables and their corresponding values in the D-optimal

Factor	Name	Units	Type	Low Actual	High Actual	Low Coded	High Coded
A	CS/Dex		Numeric	0.13	0.4	-1	1
B	Drug conc.	mg/ml	Numeric	0.5	1.5	-1	1
C	stirring rate	rpm	Numeric	800	1600	-1	1
D	temperature	C	Numeric	10	40	-1	1

Table 2. Independent and dependent variables, experimental design matrix, and results of D-optimal design

Run	Independent variables				Dependent variables		
	CS/Dex	Drug conc.	stirring rate	temperature	Z-average (d.nm)	PDI	EE (%)
1	0.13	0.5	1600	40	316.8	0.44	66.67
2	0.4	1	1200	25	208.8	0.28	79.67
3	0.4	0.5	1200	40	195.5	0.4	35.33
4	0.13	1.5	1200	40	197.4	0.37	71.33
5	0.13	1.5	800	10	300.0	0.33	88.67
6	0.4	0.5	800	10	200.7	0.39	59.67
7	0.13	1	1200	25	228.2	0.4	49.33
8	0.13	0.5	800	40	380.1	0.56	86.67
9	0.265	1.5	1200	25	200.6	0.3	73.33
10	0.4	1.5	1200	10	275.3	0.39	78.67
11	0.4	1.5	800	40	171.4	0.37	84.00
12	0.4	0.5	800	10	154.9	0.3	32.33
13	0.4	0.5	1600	10	144	0.26	53.33
14	0.13	0.5	800	40	273.8	0.48	73.67
15	0.265	1	1600	25	194.3	0.3	68.00
16	0.4	1	1600	40	205.4	0.25	89.00
17	0.4	1.5	800	40	225.9	0.32	80.67
18	0.13	0.5	1600	40	302.4	0.37	50.00
19	0.265	1	1000	25	201.9	0.41	58.67
20	0.4	1.5	1600	25	242.5	0.31	77.00
21	0.13	1.5	1600	10	237.8	0.39	66.33
22	0.265	1.5	1600	40	195.3	0.31	75.00
23	0.13	0.5	1200	10	190.9	0.34	77.00
24	0.265	0.5	1200	25	203.3	0.29	65.33
25	0.13	1.5	800	10	299.2	0.37	88.33

Table 3. Analysis of variance for D-optimal refined models

| D-optimal design	Source of variations	Sum of squares	Degree of freedom	Mean square	F value	Prob. > F	
Particle size (Z-average)	Model	67393.75	14	4813.84	5.463	0.005	Sig.
	Residual	8812.29	10	881.23			
	Lack of fit	529.43	5	105.89	0.064	0.995	Not sig.
	Pure error	8282.87	5	1656.57			
	R-Squared	0.88					
	Adj R-Squared	0.72					
	Adeq Precision	7.96					
Poly dispersity Index (PDI)	Model	0.10	14	0.01	3.149	0.037	Sig.
	Residual	0.02	10	0.002			
	Lack of fit	0.01	5	0.002	0.912	0.54	Not sig.
	Pure error	0.01	5	0.002			
	R-Squared	0.82					
	Adj R-Squared	0.56					
	Adeq Precision	7.53					
Entrapment Efficiency (EE)	Model	3869.19	10	386.92	2.612	0.049	Sig.
	Residual	2073.46	14	148.10			
	Lack of fit	1470.90	9	163.43	1.356	0.386	Not sig.
	Pure error	602.56	5	120.51			
	R-Squared	0.65					
	Adj R-Squared	0.40					
	Adeq Precision	5.33					
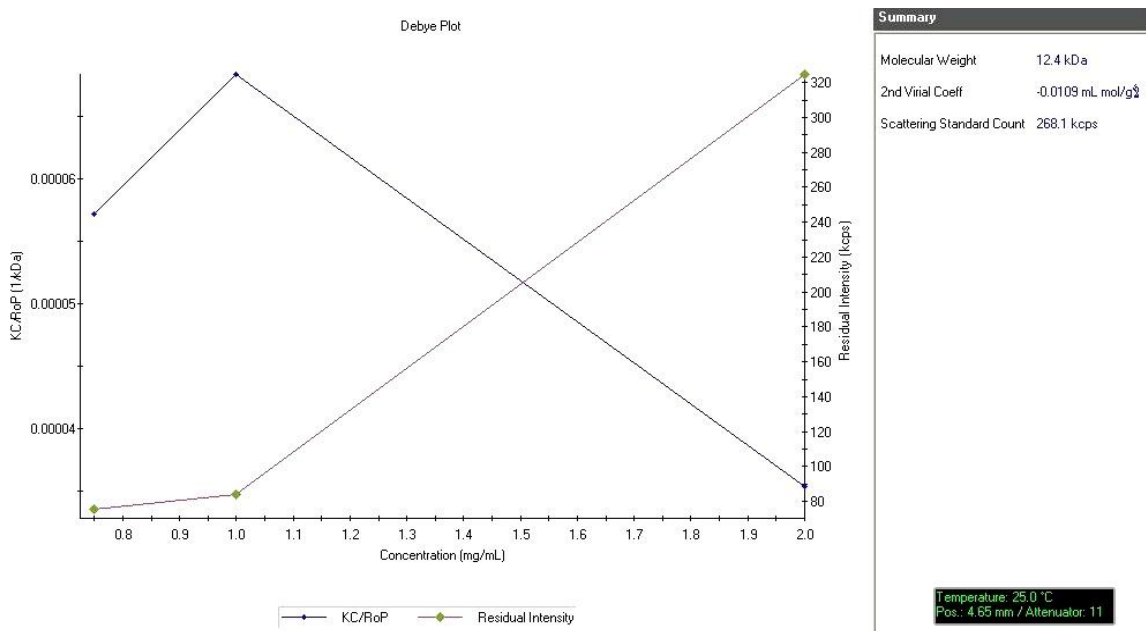
Figure 1. Debye plot of depolymerized chitosan

63

Experimental Design

The classical method of optimization based on changing one parameter at a time while keeping the others at fixed levels is laborious and time-consuming. This method requires complete series of experiments for each factor of interest. Moreover, such method does not provide means of observing possible factor interactions [27]. In contrast, experimental design offers a number of important advantages such as determination of factor effects with considerably less experimental effort and find the optimum condition for the experiment [28,29]. As shown in table 1, four relevant factors including chitosan/dextran (CS/Dex) ratio, lysozyme concentration, stirring rate, and temperature were selected as the main determinants, and the effects of factors on the final Z-average size of the particles, PDI, and entrapment efficiency (EE) of the resulting nanoparticles were studied.

Particle size optimization

The particle size was measured for all 25 experiments and fitted to a quadratic model with no detectable outliers according to the Cook's distances (Equation 2). In addition, no transformation was carried out on the data. F-value of the model indicates that the model

is significant (F = 5.46). Also, the lack of fit test revealed that it is not a significant relationship to the pure error (P value = 0.995). The relatively high R-squared (0.88) and adjusted R-squared (0.72) values revealed a good correlation between the experimental data and those of the fitted model (Table 3).

Z-average = 193.22 - 17.17 × A + 8.58 × B - 13.50 × C + 2.87 × D + 20.03 × A^2 + 8.19 × B^2 + 20.02 × C^2 - 4.33 × D^2 + 20.14 × A + 6.39 × AC - 11.29 × AD - 0.27 × BC - 38.10 × BD + 11.22 × CD

(Equation 2)

where A, B, C, and D are "CS/Dex ratio", "protein concentration", "stirring rate", and "temperature", respectively.

Figure 2 is response surface graphs based on the final model, holding two variables constant at their optimum levels, while varying the others within their experimental ranges. Figure 2a represents the response surface for the optimum levels of stirring rate and temperature. The minimum particle size was achieved when protein concentration and CS/Dex ratio were at their lowest and highest levels, respectively. Analysis of the response

revealed that there was a significant relationship between "protein concentration" and CS/Dex ratio. At the optimum points of "protein concentration" and "temperature" (Figure 2b), the minimum particle size was observed at high level of "CS/Dex ratio" and an intermediate level of "stirring rate". Analysis of the response revealed that there is no significant relationship between these factors. However, at the optimum levels of "protein concentration" and "stirring rate", there was a relationship between "CS/Dex ratio" and "temperature" factors (Figure 2c). Smaller particle sizes were achieved in lower temperatures due to the instability of electrostatic interaction between the polymers in higher temperatures. The response surface at the optimum levels of "CS/Dex ratio" and "temperature" indicates the particle size is more desirable in lower and higher levels of "protein concentration" and "stirring rate", respectively (Figure 2d). Also, "protein concentration" and "temperature" shows a significant interaction on the response (Figure 2e). As mentioned before for the polymer-polymer interaction, the temperature has also a significant effect on the protein-polymer interactions. The smaller size was achieved in the lower levels of both "temperature" and "protein concentration". The response surface at the optimum levels of "CS/Dex ratio" and

"protein concentration" elucidates the smaller particle sizes were obtained at lower level of "temperature" and higher level of "stirring rate". It must be noted that in lower temperatures, the effect of stirring rate was negligible (Figure 2f).

Poly dispersity index optimization

PDI was obtained for all 25 experiments and fitted to a quadratic model with no detectable outliers (Equation 3). In addtion, no transformation was applied on the data. The F-value of the model ($F = 3.15$) indicates that the model is significant and lack of fit test did not reveal a significant difference relative to the pure error (P value = 0.539). The proper R-squared (0.82) and adjusted R-squared (0.56) values implied a good relationship between the experimental data and those of the fitted model (Table 3).

$$PDI = 0.34 - 0.025 \times A - 2.913 \times 10^{-3} \times B - 0.032 \times C + 0.013 \times D + 5.661 \times 10^{-3} \times A^2 - 0.019 \times B^2 - 5.753 \times 10^{-3} \times C^2 + 0.036 \times D^2 + 9.342 \times 10^{-3} \times AB - 0.014 \times AC - 0.019 \times AD + 0.023 \times BC - 0.035 \times BD - 0.021 \times CD$$

(Equation 3)

Where A, B, C, and D are "CS/Dex ratio", "protein concentration", "stirring rate", and "temperature", respectively.

The minimum PDI was achieved when "protein concentration" and "CS/Dex ratio" were at their lowest and highest levels, respectively. Analysis of the response at the different levels revealed that there was a remarkable interaction between these factors (Figure 3a). This phenomenon could be explained as the same for particle size optimization. At the optimum levels of "protein concentration" and "temperature", the minimum PDI was obtained at high levels of both "CS/Dex ratio" and "stirring rate" (Figure 3b). Nonetheless, analysis of the response revealed that there was no significant interaction between these factors. Response surface at the optimum levels of "protein concentration" and "stirring rate" demonstrates the PDI is smallest at high level of "CS/Dex ratio" and intermediate level of "temperature" (Figure 3c). Response surface at the optimum levels of "CS/Dex ratio" and "temperature" shows the PDI was smaller at lower and higher levels of "protein concentration" and "stirring rate" (Figure 3d). However, it was not detected a remarkable interaction between these factors. "Protein concentration" and "temperature" show an important interaction at the optimum levels of "CS/Dex ratio" and "stirring rate" (Figure 3e). Lower PDI values were obtained at both lower and higher levels of "temperature" and "protein concentration"

factors. In fact, the temperature has also a significant effect on the protein-polymer interactions. Finally, the response surface at the optimum levels of "CS/Dex ratio" and "protein concentration" indicates the PDI is more desirable at low to intermediate levels of "temperature" and high level of "stirring rate" (Figure 3f).

Entrapment efficiency optimization

Entrapment efficiency was calculated for all 25 experiments and fitted to a 2FI model with no detectable outliers (Equation 4). In addtion, no transformation was applied on the raw data. The F-value of the model (F = 2.61) indicates that the model is significant. Also, the lack of fit test revealed that there is no significant difference relative to the pure error (P value = 0.651). The relatively acceptable R-squared (0.65) and adjusted R-squared (0.40) values indicated there is a good correlation between the experimental data and those of the fitted models (Table 3).

$$EE = 68.79 - 2.23 \times A + 8.07 \times B - 3.09 \times C - 0.64 \times D + 8.70 \times AB + 8.50 \times AC + 2.77 \times AD - 0.85 \times BC + 1.64 \times BD + 1.79 \times CD$$

(Equation 4)

Where A, B, C, and D are "CS/Dex ratio", "protein concentration", "stirring rate", and "temperature", respectively.

Response surface at the optimum levels of "stirring rate" and "temperature" showed the maximum entrapment efficiency of the protein was occurred when "protein concentration" and "CS/Dex ratio" are at the highest levels (Figure 4a). In the other words, the more protein concentration led to the more entrapment efficiency. At the optimum levels of "protein concentration" and "temperature", the maximum entrapment of the protein in the nanoparticles was seen at the lowest levels of "CS/Dex ratio" and "stirring rate" factors (Figure 4b). Similarly, at the optimum points of "protein concentration" and "stirring rate", the entrapment efficiency has a highest value when "temperature" and "CS/Dex ratio" factors are at the lowest levels (Figure 4c). At the optimum levels of "CS/Dex ratio" and "temperature", entrapment efficiency was highest at higher and lower levels of "protein concentration" and "stirring rate", respectively (Figure 4d). The response surface graph at the optimum levels of "CS/Dex ratio" and "stirring rate" illustrates that the higher protein entrapment is obtianed at higher levels of both "temperature" and "protein concentration" factors (Figure 4e). Moreover, data revealed the protein

entrapment was higher at lower levels of both "temperature" and "stirring rate" when "CS/Dex ratio" and "protein concentration" factors are at the optimum levels (Figure 4f).

Multi-criteria optimization

Obtainnig the experimental conditions which result in the best response is the main goal of optimization studies. However, dependent variables may be have contradictory effects to each other, and therefore, it is necessary to determine such interactions. To solve this issue, desirability functions are utilized in a process known as multi-criteria optimization [30]. This approach, Derringer's desirability (D) is calculated uisng the geometric mean, weighted or otherwise, of the individual desirability functions (Equation 5) [31].

$$D = [d_1 \times d_2 \times \ldots \times d_n]^{1/n} \qquad 0 < D < 1$$
(Equation 5)

Where "n" is the number of responses in the measure, and "d_i" is the individual desirability function of each response obtained from the transformation of the individual response in each experiment. The scale of the individual desirability function ranges between $d_i = 0$ for a completely undesired response, and $d_i = 1$ for a fully desired response. For a value of D close to 1, response values are near the target values.

67

The optimum responses were assumed as follow: (a) minimum values for the particle size and PDI and (b) highest entrapment efficiency of the protein in the nanoparticles. The optimum conditions was identified as a CS/Dex ratio of 0.37 in a solution containing of 1.5 mg/mL lysosyme with 1600 rpm stirring at 32.72˚C. The predicted optimal particle size, PDI, and the protein entrapment efficiency corresponding to these values were calculated as 217.5 d.nm, 0.26, and 87.06 %, respectively. This condition corresponds to the maximum desirability functions within the range of experimental values (D = 0.857). To confirm the model adequacy, five additional experiments using the optimum condition were performed. The good agreement between the predicted and experimental results verified the validity of the models as well as the optimum condition for lysosyme-loaded nanoparticle preparation.

Morphological characterization

Morphological study using SEM and AFM revealed that the optimized nanoparticles have a spherical shape and a smooth surface (Figure 5).

In vitro release

The release profile of protein from the nanoparticles is shown in figure 6. There was an initial burst release about 60 % of loaded protein in the first 7 h. After 24 h, the release rate was reduced and followed by a linear phase between 2nd and 10th days.
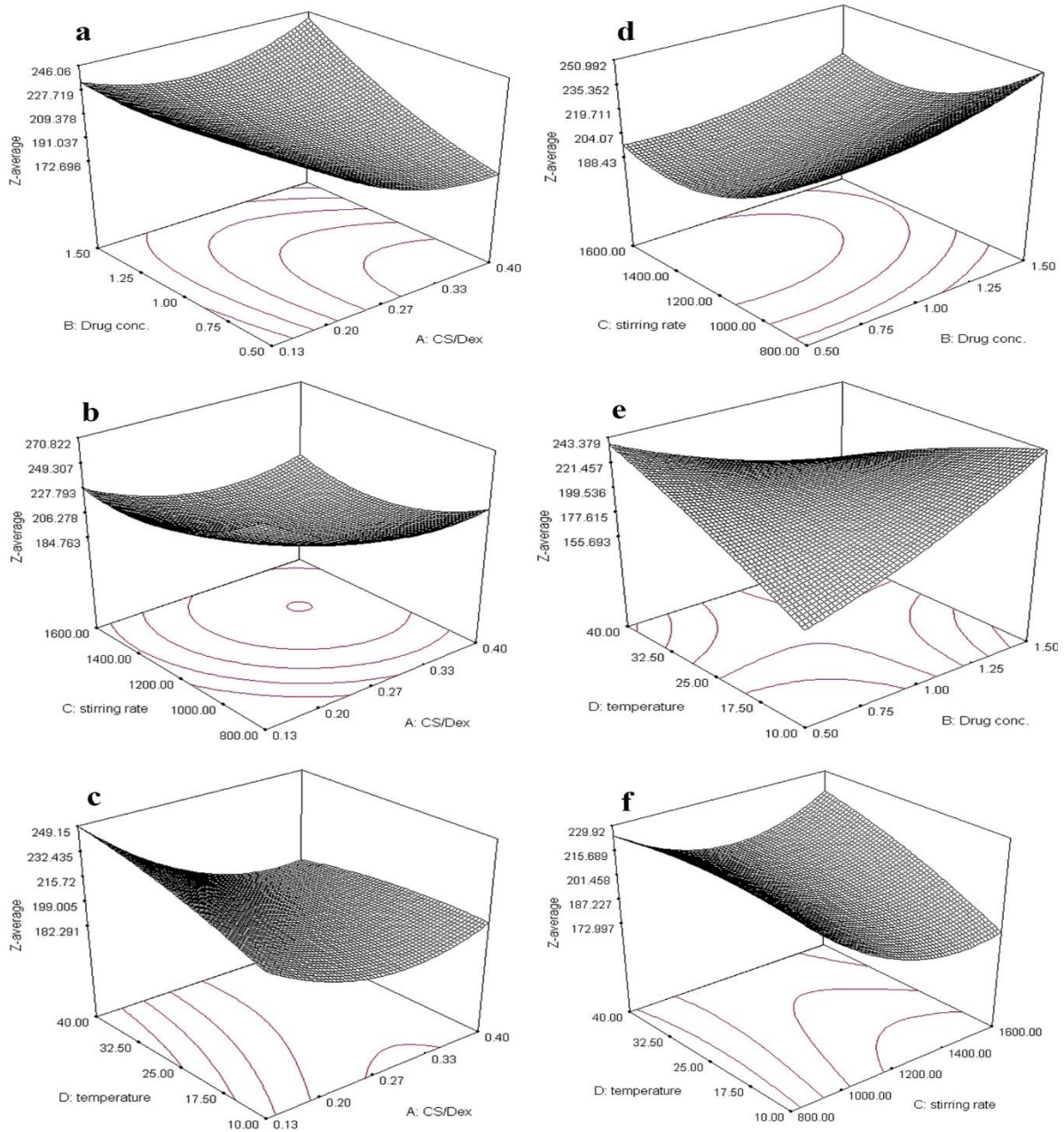
68

Figure 2. Response surface of particle size (Z-average): (a)–(f) fixed "stirring rate" and "temperature", "protein concentration" and "temperature", "protein concentration" and "stirring rate", "CS/Dex ratio" and "temperature", "CS/Dex ratio" and "stirring rate", "CS/Dex ratio" and "protein concentration" levels at their optimum points, respectively.
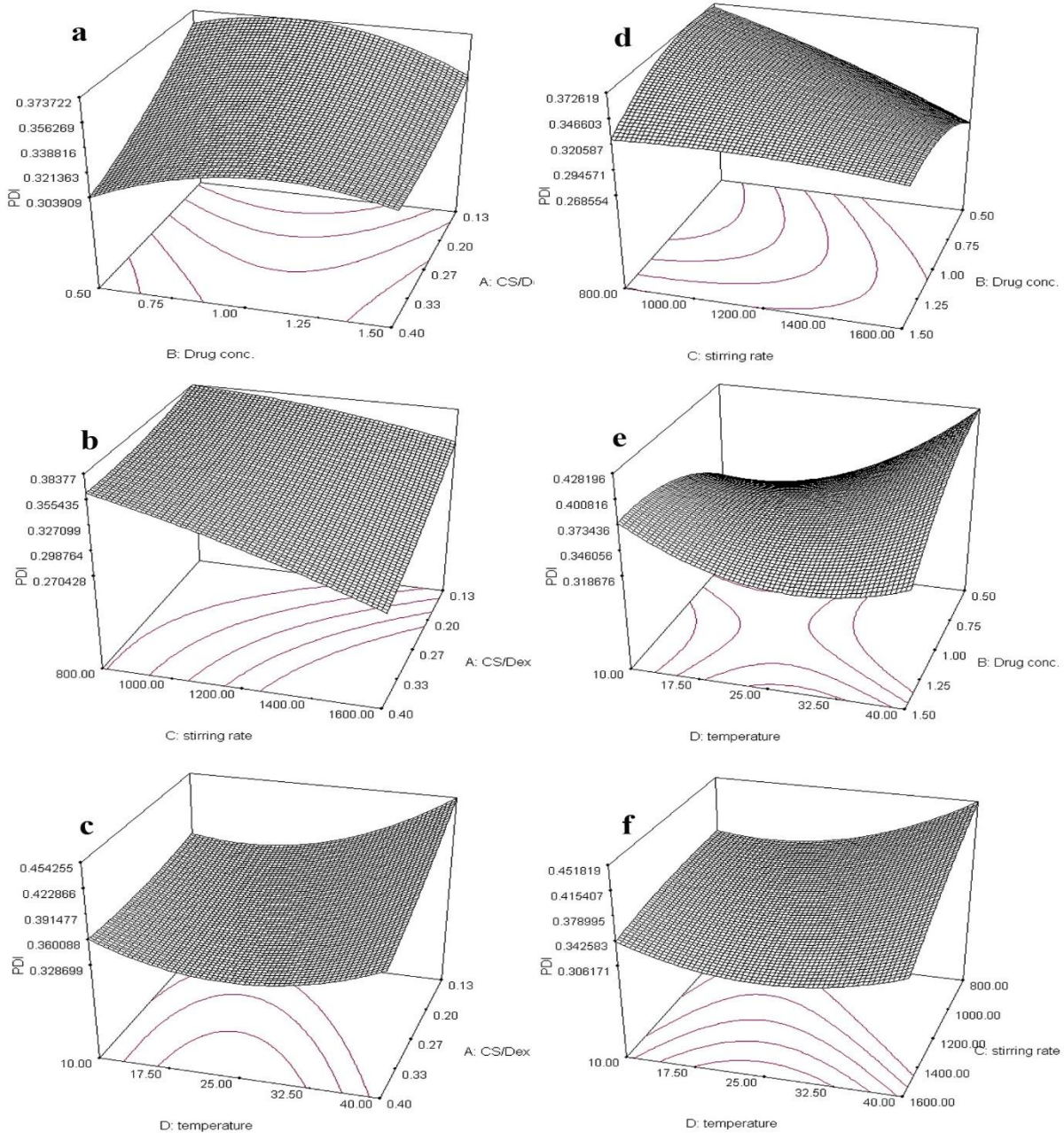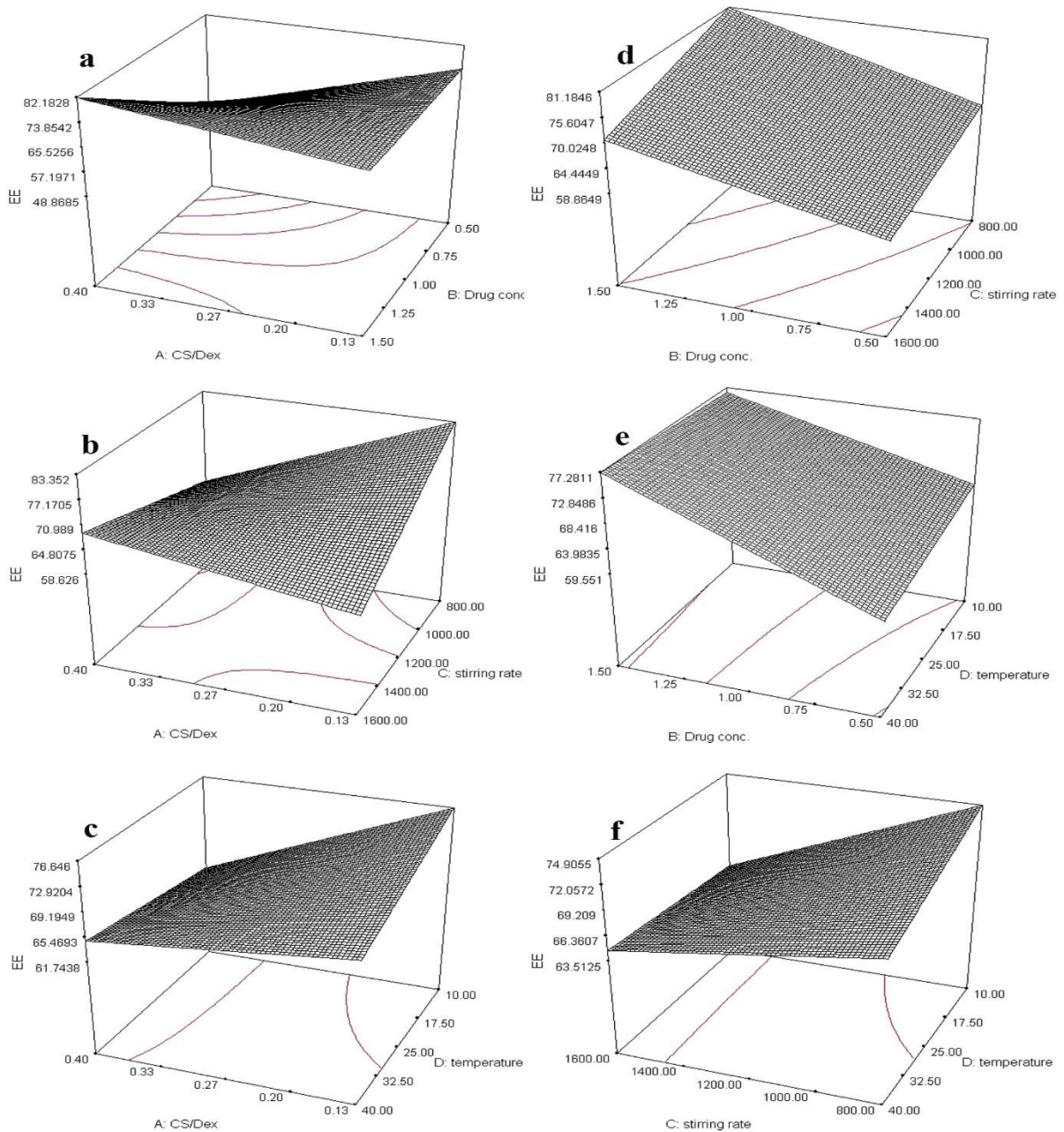
70

Figure 3. Response surface of polydispersity index (PDI): (a)–(f) fixed "stirring rate" and "temperature", "protein concentration" and "temperature", "protein concentration" and "stirring rate", "CS/Dex ratio" and "temperature", "CS/Dex ratio" and "stirring rate", "CS/Dex ratio" and "protein concentration" levels at their optimum points, respectively.
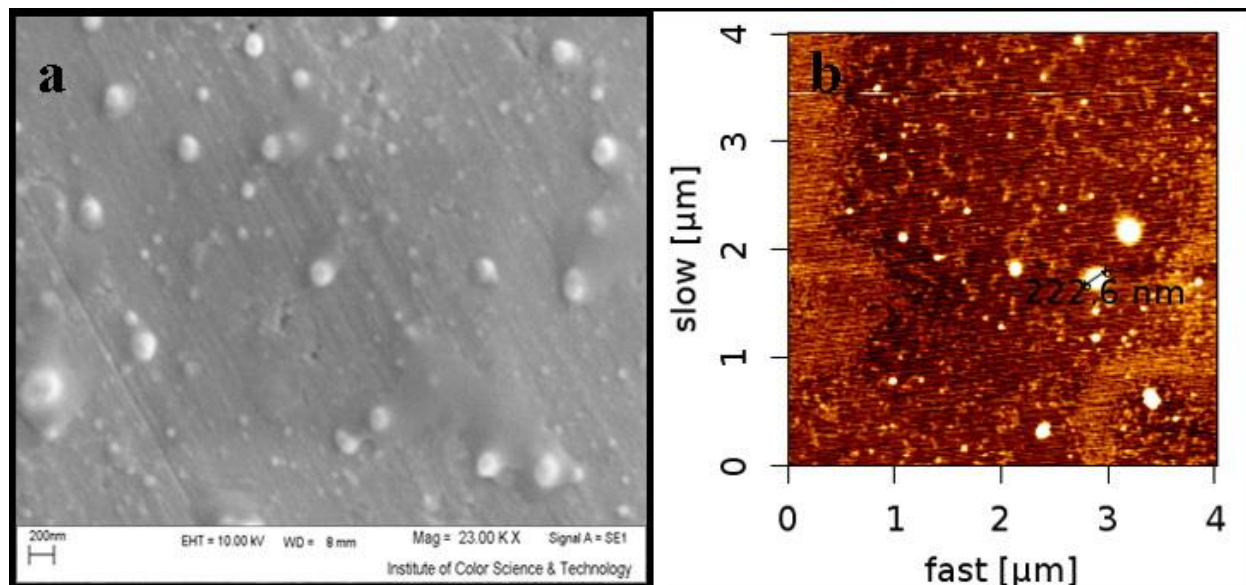
71

Figure 4. Response surface of entrapment efficiency (EE): (a)–(f) fixed "stirring rate" and "temperature", "protein concentration" and "temperature", "protein concentration" and "stirring rate", "CS/Dex ratio" and "temperature", "CS/Dex ratio" and "stirring rate", "CS/Dex ratio" and "protein concentration" levels at their optimum points, respectively.

72

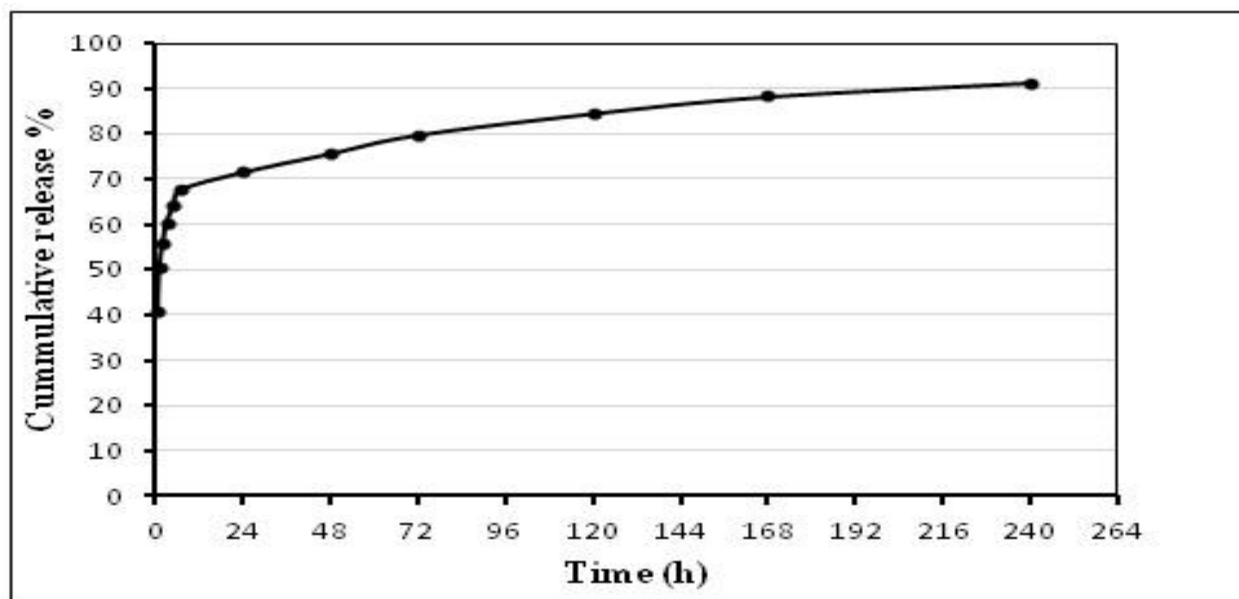**Figure 5**. (a) SEM image of optimum nanoparticles (b) AFM topographic images of optimum nanoparticles

Figure 6. Release profile of the protein from CS/Dex nanoparticles.

73

DISCUSSION

In the current study, the effect of different parameters (polymer ratio, protein concentration, stirring rate, and temperature) was evaluated on the preparation of lysozyme loaded dextran-chitosan nanoparticles using response surface methodology. Experiments on different molecular weights of chitosan revealed that the nanoparticles with less size and high encapsulation efficiency were achieved when low molecular weight of chitosan was used. This explains by this fact that the encapsulation efficiency of chitosan is inversely proportional to the molecular weight. In more precise terms, depolymerization of chitosan makes more exposed amino groups [32].

The effect of polymer ratio on the size of nanoparticles was investigated by maintaining the amount of chitosan at a constant level. Since the negative charge of dextran monomer was greater than the positive charge of chitosan monomer, increasing CS/Dex ratio reduces the particle size until an optimum point. At this point, polymers make a stable complex and after that, the larger particles were formed [33, 34]. Protein concentration showed a direct effect on the size of nanoparticles. On the other hand, an increase in protein concentration leads to an increase in the size of

nanoparticles. This could be well explained by entering of protein molecules to the nanoparticle structure during synthesis [35]. Similarly, the temperature has also a direct effect on the size and PDI of the prepared nanoparticles. Since the mechanism of nanoparticle formation is based on an electrostatic interaction between oppositely charged polymers, more stable interactions are formed at lower temperatures, and thereby smaller nanoparticles with a narrow range of size distribution were obtained. In contrast to the temperature and protein concentration, the stirring rate exhibited an inverse effect on both size and PDI responses. As the speed increases, the collisions between the particles are more occurring, and thereby the particles are uniformly formed of protein and polymers in low particle size [36].

The CS/Dex ratio has a reciprocal effect on the encapsulation of the protein. Since lysozyme has a positive charge in the reaction, it interferes with electrostatic interaction between the oppositely charged polymers. By increasing the chitosan amount, a competition was occurred between chitosan and the protein to interact with the dextran molecules. Therefore, the probability of presence of the protein was reduced in the nanoparticle structures [37, 38]. Inversely, with an increase in the protein concentration,

the competition between chitosan and lysozyme for binding to the anionic polymer pushes towards the protein. Therefore, nanoparticles encapsulate more protein molecules [39].

The temperature had an inverse effect on the encapsulation efficiency. But the effect was negligible at higher protein concentrations. Temperature attenuates the electrostatic interaction between the protein and the polymer and therefore reduces the encapsulation yield. But at lower temperatures as well as high protein concentrations, the interaction is more stable and the encapsulation efficiency is high [40]. Likewise, stirring had a reciprocal effect on the encapsulation yield. As the stirring speed increases, the possibility of protein entrance into the nanoparticle structures reduces, and thereby the encapsulation efficiency decreases.

Encapsulated lysozyme showed a burst release about 60 % of loaded protein in the first 7 h followed by a sustained release in the physiological condition. The initial burst release might be due to release of loosely adsorbed protein molecules at the surface of nanoparticles. The sustained release pattern could be explained by diffusion of lysozyme from CS/Dex nanoparticles due to swelling/degradation [41].

CONCLUSION

In conclusion, our study demonstrated the benefits of D-optimal design to determine the important factors, as well as the optimum conditions for the nanoparticle preparation. By using such approach, more efficient size and encapsulation yield was achieved.

REFERENCES

[1]. Tan ML, Choong PF, Dass CR. Recent developments in liposomes, microparticles and nanoparticles for protein and peptide drug delivery. *Peptides*, 2010. 31(1): 184-93.

[2]. Jitendra P, Bansal S, Banik A. Noninvasive routes of proteins and peptides drug delivery. *Indian J Pharm Sci,* 2011. 73(4): 367.

[3]. Patel A, Cholkar K, Mitra AK. Recent developments in protein and peptide parenteral delivery approaches. *Ther Deliv,* 2014. 5(3): 337-65.

[4]. Shantha Kumar T, Soppimath K, Nachaegari S. Novel delivery technologies for protein and peptide therapeutics. *Curr Pharm Biotechnol*, 2006. 7(4): 261-76.

[5]. Pisal DS, Kosloski MP, Balu-Iyer SV. Delivery of therapeutic proteins. *J Pharm Sci*, 2010. 99(6): 2557-75.

[6]. Tiyaboonchai W. Chitosan nanoparticles: a promising system for drug delivery. Naresuan University J: *Sci Technol, 2013. 11*(3): 51-66.

[7]. Cooper C. Polyelectrolyte–protein complexes. *Curr Opin Colloid Interface Sci*, 2005. 10(2): 52-78.

[8]. Chen Y, Mohanraj VJ, Parkin JE. Chitosan-dextran sulfate nanoparticles for delivery of an anti-angiogenesis peptide. *Lett Peptide Sci*, 2003. 10(5-6): 621-629.

[9]. Irache JM. Optimization and *in vitro* stability of legumin nanoparticles obtained by a coacervation method. *Int J Pharm,* 1995. 126(1-2): 103-9.

[10]. Briones AV, Sato T. Encapsulation of glucose oxidase (GOD) in polyelectrolyte complexes of chitosan–carrageenan. *React Funct Polym*, 2010. 70(1): 19-27.

[11]. Hamman JH. Chitosan based polyelectrolyte complexes as potential carrier materials in drug delivery systems. *Mar drugs*, 2010. 8(4): 1305-22.

[12]. Sarmento B. Development and comparison of different nanoparticulate polyelectrolyte complexes as insulin carriers. *Int J Pept Res Ther,* 2006. 12(2): 131-38.

[13]. Vasilescu A. Aptamer-based electrochemical sensing of lysozyme. *Chemosensors,* 2016. 4(2): 10-15.

[14]. Blake C. Crystallographic studies of the activity of hen egg-white lysozyme. *Proc R Soc Lond,* 1967. 167(1009): 378-88.

[15]. Calvo P, Vila-Jato J, Alonso M. Effect of lysozyme on the stability of polyester nanocapsules and nanoparticles: stabilization approaches. *Biomaterials*, 1997. 18(19): 1305-10.

[16]. Cai, C. Charged nanoparticles as protein delivery systems: a feasibility study using lysozyme as model protein. *Eur J Pharm Biopharm*, 2008. 69(1): 31-42.

[17]. Han SK. Hydrophilized poly (lactide-co-glycolide) nanoparticles with core/shell structure for protein delivery. *Sci Technol Adv Mater*, 2005. 6(5): 468-72.

[18]. Moghaddam FA, Atyabi F, Dinarvand R. Preparation and *in vitro* evaluation of mucoadhesion and permeation enhancement of thiolated chitosan-pHEMA core-shell nanoparticles. *Biol Med*, 2009. 5(2): 208-15.

[19]. Földényi R. Study of sorption of two sulfonylurea type of herbicides and their additives on soils and soil components. *J Environ Sci Health*, 2013. 48(9): 758-66.

[20]. Mattison K, Kaszuba M. Measuring absolute protein molecular weight: Is multiangle instrumentation absolutely

essential? *Am Biotechnol Lab,* 2003. 21(7): 28-29.

[21]. Leiro J. A factorial experimental design for investigation of the effects of temperature, incubation time, and pathogen-to-phagocyte ratio on *in vitro* phagocytosis by turbot adherent cells. *Comp Biochem Physiol Pharmacol, Toxicol Endocrinol,* 1995. 112(2): 215-20.

[22]. Siso MI. Microfungus-yeast mixed cultures in the degradation of amylaceous wastes. I: Interactions affecting amylolytic activity. *Biotechnol lett,* 1988. 10(6): 431-36.

[23]. Huang M, Berkland C. Controlled release of Repifermin® from polyelectrolyte complexes stimulates endothelial cell proliferation. *J Pharm Sci,* 2009. 98(1): 268-80.

[24]. Huang M. Polyelectrolyte complexes stabilize and controllably release vascular endothelial growth factor. *Biomacromolecules,* 2007. 8(5): 1607-14.

[25]. Delair T. Colloidal polyelectrolyte complexes of chitosan and dextran sulfate towards versatile nanocarriers of bioactive molecules. *Eur J Pharm Biopharm,* 2011. 78(1): 10-18.

[26]. Van de Weert M, Hennink WE, Jiskoot W. Protein instability in poly (lactic-co-glycolic acid) microparticles. *Pharm Res*, 2000. 17(10): 1159-67.

[27]. Azadi A. Preparation and optimization of surface-treated methotrexate-loaded nanogels intended for brain delivery. *Carbohydr Polym*, 2012. 90(1): 462-71.

[28]. Kincl M, Turk S, Vrečer F. Application of experimental design methodology in development and optimization of drug release method. *Int J Pharm,* 2005. 291(1-2): 39-49.

[29]. Hamidi M. Taguchi orthogonal array design for the optimization of hydrogel nanoparticles for the intravenous delivery of small-molecule drugs. *J Appl Polym Sci,* 2012. 126(5): 1714-24.

[30]. Deming SN. Multiple-criteria optimization. *J Chromatogr*, 1991. 550: 15-25.

[31]. Derringer G, Suich R. Simultaneous optimization of several response variables. *J Qual Techno*l, 1980. 12(4): 214-19.

[32]. Sabnis S, Block LH. Chitosan as an enabling excipient for drug delivery systems: Molecular modifications. *Int J Biol Macromolecules*, 2000. 27(3): 181-86.

[33]. Chen Y. Designing chitosan-dextran sulfate nanoparticles using charge ratios. *Pharm Sci Tech,* 2007. 8(4): 131-39.

[34]. Mitra S. Tumour targeted delivery of encapsulated dextran–doxorubicin conjugate using chitosan nanoparticles as carrier. *J Control Release*, 2001. 74(1-3): 317-23.

[35]. Sarmento B. Development and characterization of new insulin containing polysaccharide nanoparticles. Colloids and Surfaces B: *Biointerfaces,* 2006. 53(2): 193-202.

[36]. Sarmento B. Insulin-loaded nanoparticles are prepared by alginate ionotropic pre-gelation followed by chitosan polyelectrolyte complexation. *J Nanosci Nanotechnol,* 2007. **7**(8): 2833-41.

[37]. Calvo P. Chitosan and chitosan/ethylene oxide-propylene oxide block copolymer nanoparticles as novel carriers for proteins and vaccines. *Pharm Res,* 1997. 14(10): 1431-36.

[38]. Gan Q, Wang T. Chitosan nanoparticle as protein delivery carrier—systematic examination of fabrication conditions for efficient loading and release. Colloids and Surfaces B: *Biointerfaces*, 2007. 59(1): 24-34.

[39]. Pan Y. Bioadhesive polysaccharide in protein delivery system: chitosan nanoparticles improve the intestinal absorption of insulin *in vivo*. *Int J Pharm*, 2002. 249(1-2): 139-47.

[40]. Fan W. Formation mechanism of monodisperse, low molecular weight chitosan nanoparticles by ionic gelation technique. *Colloids Sur B: Biointerfaces*, 2012. 90: 21-27.

[41]. Jingou J. Preparation, characterization of hydrophilic and hydrophobic drug in combine loaded chitosan/cyclodextrin nanoparticles and *in vitro* release study. *Colloids Sur B: Biointerfaces*, 2011. 83(1): 103-107.